Int J Adv Manuf Technol (2018) 94:1451–1460
DOI 10.1007/s00170-017-0957-y

ORIGINAL ARTICLE

An efficient experimental approach to identify tool point FRF by improved receptance coupling technique

Jingping Liao[1] · **Dingwen Yu**[1,2] · **Jianfu Zhang**[1,2] · **Pingfa Feng**[1,2,3] · **Zhijun Wu**[1,2]

Received: 15 March 2017 / Accepted: 14 August 2017 / Published online: 29 August 2017
© Springer-Verlag London Ltd. 2017

Abstract Chatter can be predicted and avoided through the chatter stability lobe, which is computed by dynamic response (frequency response function) at the tool point. Modal impact testing is time-consuming and inefficient, which is not suitable for tool point dynamic prediction. On the contrary, receptance coupling method can efficiently identify the tool point dynamic by combining the full (translational and rotational) receptance matrix of spindle-holder assembly with numerical or analytical model of any attached free-free tool. Generally, it is difficult to directly obtain the rotational receptances of spindle-holder assembly. This paper proposes an efficient experimental method which deduces the rotational receptances from translational receptances on a single experimental setup by improved receptance coupling technique. One main advantage of this method is to further reduce required impact tests and increase efficiency of tool point dynamic prediction. Besides, a wider application of the proposed method can be achieved. The presented approach is experimentally verified and compared with the state-of-the-art methods.

✉ Jianfu Zhang
zhjf@tsinghua.edu.cn

[1] State Key Laboratory of Tribology & Institute of Manufacturing Engineering, Department of Mechanical Engineering, Tsinghua University, Beijing 100084, People's Republic of China

[2] Beijing Key Lab of Precision/Ultra-precision Manufacturing Equipments and Control, Tsinghua University, Beijing 100084, People's Republic of China

[3] Graduate School at ShenZhen, Tsinghua University, ShenZhen 518055, China

Keywords Milling · Dynamics · Receptance coupling technique · Frequency response function · Experimental approach

1 Introduction

High-speed machining is widely used in modern industries, for its ability to gain better surface quality and higher material removal rate (MRR) than the conventional-speed machining. Unstable machining, i.e., chatter, is one of the major limitations to successful application of high-speed machining, because it can significantly influence the machine tool life and machined surface quality [1–4]. Thus, it is important to accurately predict and effectively avoid chatter in high-speed machining. The well-known stability lobe diagram is a useful tool to achieve chatter prediction and avoidance. In the stability lobe diagram, a function of spindle speed and axial depth of cut can be used to separate the stable cutting zone and the unstable one. The tool point frequency response function (FRF) is the important precondition for the development of this stability lobe diagram [5, 6].

Traditionally, the tool point FRF can be obtained by an experimental method, which uses an impact hammer and a low-mass accelerometer to excite the tool point and measure the resulting vibration signals, respectively. Hammer impact testing requires both proper technique and appropriate intensity, which is not a random procedure [7]. Improper hammer impact may lead to inaccurate results. Besides, due to the enormous number of tool/holder/spindle combinations, the impact testing method may be time-consuming and inefficient. Hence, further reduction of hammer impact times is of great

significance to improve prediction efficiency. To overcome the disadvantages of the hammer impact testing method, a theoretical method named RCSA (Receptance Coupling Substructure Analysis) was proposed by Schmitz et al. [8]. In RCSA, the assembly FRF is predicted by coupling its substructure FRFs through appropriate joint dynamics. Thus, one of the important influencing factors involved in application of RCSA is accurate identification of substructure receptances [9–13].

In recent decades, many investigations have been carried out on identification of substructure dynamics. Ertürk [11] analytically modeled the tool-holder-spindle assembly dynamics using Timoshenko beam theory and receptance coupling technique to predict the tool point FRF. In the first-generation RCSA method, Schmitz et al. [8] divided the tool-holder-spindle assembly into two substructures: the tool and holder/spindle combination. The tool FRFs were analytically derived and only the translational FRFs of the holder/spindle combination were taken into account, neglecting the rotational dynamics. It has been demonstrated that the substructure rotational dynamic responses have a significant influence on system response [14]. Due to the high cost and poor accuracy of angular response transducers [15], it is difficult to directly measure the rotational dynamics. The common method to obtain the rotational FRFs is to derive such information from translational FRF measurements using finite difference technique [14]. Schmitz et al. [16] determined all four spindle-holder base subassembly receptances by applying a second-order backward finite difference method in the second-generation RCSA method. Liu [15] made use of rotational FRFs, which were derived from translational FRFs based on finite difference technique, to identify the spindle-holder joint contact stiffness. Albertelli [17] presented an improved RCSA approach by proposing a new expression of rotation-to-moment receptance component based on finite difference calculation. However, the key to successful application of finite difference technique is selecting an appropriate distance value between the measurement points [18].

Kumar [19] proposed an alternative method that avoided errors in finite difference approximation. In this method, each mode in the measured translational FRF was described by the closed-form receptance expression for Euler-Bernoulli (E-B) cantilever beam. Once the E-B beam properties were determined, the other receptance components could be obtained with theoretical formulas. An extended study on this method was completed by Ganguly [20]. Park et al. [21] proposed an algorithm to extract rotational dynamics of the spindle-holder combination based on solving non-linear translational receptance equations. Two blank cylinders with different lengths were inserted into the holder, and three impacts were conducted using only one accelerometer to identify the corresponding translational FRFs. This method was also adopted by other researchers [22, 23]. However, its main drawback is introducing additional test setups and making RCSA less attractive. The number of experiments directly affects the machine downtime. To improve the prediction efficiency of receptance coupling technique, Montevecchi et al. [24] presented an improved RCSA method which could decrease the number of impact measurements. The proposed approach conducted experiments on a single test setup using two accelerometers. Two impact tests were conducted to obtain translational FRFs, which were processed by the proposed inverse receptance coupling technique to compute the rotational dynamic responses of spindle-holder assembly.

This paper proposes an improved RCSA method for efficient prediction of tool point FRF. The presented approach conducts only one impact test using two accelerometers on a single test setup to obtain the required translational FRFs. The resulting FRFs are then used to compute rotational dynamics based on the proposed inverse receptance coupling method. The extracted translational and rotational dynamics of spindle-holder assembly can be stored as a constant database, which can be used to evaluate the tool point FRF by analytically coupling them with any attached free-free tool dynamics. The main advantage of this method is further reducing the number of required measurements, hence decreasing machine downtime and improving the prediction efficiency of the RCSA method. Besides, a wider range of tool length for tool point FRF prediction can be achieved due to elimination of impact at the coupling joint location. The accuracy of the proposed approach is experimentally verified.

2 Improved receptance coupling technique

The objective of the receptance coupling technique is to accurately and efficiently compute tool point FRF. The general substructure receptance coupling model for the tool point FRF is shown in Fig. 1. *SH* is the spindle-holder assembly with inserted short blank cylinder, *T* is the free-free tool, and *A* stands for the whole tool-holder-spindle assembly. Point 1 is the tool point, point 2 is the additional point, and point 3 is the joint location which couples *SH* and *T*. Once the dynamic responses (i.e., rotational and translational receptances) of substructure *SH* at point 3 are identified, the tool

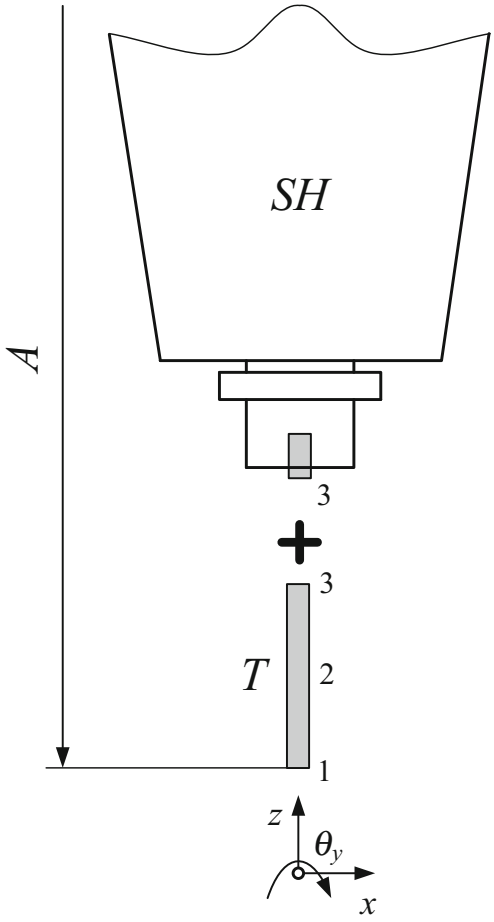

Fig. 1 Substructures and system

point FRF can be predicted by analytically coupling them to any attached tool dynamics.

Based on the classical receptance coupling technique, the displacement vector at point i (i.e., 1, 2, 3) for each substructure can be expressed as, respectively,

$$\begin{Bmatrix} x_{SH3} \\ \theta_{SH3} \end{Bmatrix} = \begin{bmatrix} g_{SH3x3f} & g_{SH3x3m} \\ g_{SH3\theta3f} & g_{SH3\theta3m} \end{bmatrix} \begin{Bmatrix} f_{SH3} \\ m_{SH3} \end{Bmatrix} \tag{1}$$

$$\begin{Bmatrix} x_{T1} \\ \theta_{T1} \end{Bmatrix} = \begin{bmatrix} g_{T1x3f} & g_{T1x3m} \\ g_{T1\theta3f} & g_{T1\theta3m} \end{bmatrix} \begin{Bmatrix} f_{T3} \\ m_{T3} \end{Bmatrix} + \begin{bmatrix} g_{T1x2f} & g_{T1x2m} \\ g_{T1\theta2f} & g_{T1\theta2m} \end{bmatrix} \begin{Bmatrix} f_{T2} \\ m_{T2} \end{Bmatrix} + \begin{bmatrix} g_{T1x1f} & g_{T1x1m} \\ g_{T1\theta1f} & g_{T1\theta1m} \end{bmatrix} \begin{Bmatrix} f_{T1} \\ m_{T1} \end{Bmatrix} \tag{2}$$

$$\begin{Bmatrix} x_{T2} \\ \theta_{T2} \end{Bmatrix} = \begin{bmatrix} g_{T2x3f} & g_{T2x3m} \\ g_{T2\theta3f} & g_{T2\theta3m} \end{bmatrix} \begin{Bmatrix} f_{T3} \\ m_{T3} \end{Bmatrix} + \begin{bmatrix} g_{T2x2f} & g_{T2x2m} \\ g_{T2\theta2f} & g_{T2\theta2m} \end{bmatrix} \begin{Bmatrix} f_{T2} \\ m_{T2} \end{Bmatrix} + \begin{bmatrix} g_{T2x1f} & g_{T2x1m} \\ g_{T2\theta1f} & g_{T2\theta1m} \end{bmatrix} \begin{Bmatrix} f_{T1} \\ m_{T1} \end{Bmatrix} \tag{3}$$

$$\begin{Bmatrix} x_{T3} \\ \theta_{T3} \end{Bmatrix} = \begin{bmatrix} g_{T3x3f} & g_{T3x3m} \\ g_{T3\theta3f} & g_{T3\theta3m} \end{bmatrix} \begin{Bmatrix} f_{T3} \\ m_{T3} \end{Bmatrix} + \begin{bmatrix} g_{T3x2f} & g_{T3x2m} \\ g_{T3\theta2f} & g_{T3\theta2m} \end{bmatrix} \begin{Bmatrix} f_{T2} \\ m_{T2} \end{Bmatrix} + \begin{bmatrix} g_{T3x1f} & g_{T3x1m} \\ g_{T3\theta1f} & g_{T3\theta1m} \end{bmatrix} \begin{Bmatrix} f_{T1} \\ m_{T1} \end{Bmatrix} \tag{4}$$

$$\begin{Bmatrix} x_{A1} \\ \theta_{A1} \end{Bmatrix} = \begin{bmatrix} g_{A1x3f} & g_{A1x3m} \\ g_{A1\theta3f} & g_{A1\theta3m} \end{bmatrix} \begin{Bmatrix} f_{A3} \\ m_{A3} \end{Bmatrix} + \begin{bmatrix} g_{A1x2f} & g_{A1x2m} \\ g_{A1\theta2f} & g_{A1\theta2m} \end{bmatrix} \begin{Bmatrix} f_{A2} \\ m_{A2} \end{Bmatrix} + \begin{bmatrix} g_{A1x1f} & g_{A1x1m} \\ g_{A1\theta1f} & g_{A1\theta1m} \end{bmatrix} \begin{Bmatrix} f_{A1} \\ m_{A1} \end{Bmatrix} \tag{5}$$

$$\begin{Bmatrix} x_{A2} \\ \theta_{A2} \end{Bmatrix} = \begin{bmatrix} g_{A2x3f} & g_{A2x3m} \\ g_{A2\theta3f} & g_{A2\theta3m} \end{bmatrix} \begin{Bmatrix} f_{A3} \\ m_{A3} \end{Bmatrix} + \begin{bmatrix} g_{A2x2f} & g_{A2x2m} \\ g_{A2\theta2f} & g_{A2\theta2m} \end{bmatrix} \begin{Bmatrix} f_{A2} \\ m_{A2} \end{Bmatrix} + \begin{bmatrix} g_{A2x1f} & g_{A2x1m} \\ g_{A2\theta1f} & g_{A2\theta1m} \end{bmatrix} \begin{Bmatrix} f_{A1} \\ m_{A1} \end{Bmatrix} \tag{6}$$

$$\begin{Bmatrix} x_{A3} \\ \theta_{A3} \end{Bmatrix} = \begin{bmatrix} g_{A3x3f} & g_{A3x3m} \\ g_{A3\theta3f} & g_{A3\theta3m} \end{bmatrix} \begin{Bmatrix} f_{A3} \\ m_{A3} \end{Bmatrix} + \begin{bmatrix} g_{A3x2f} & g_{A3x2m} \\ g_{A3\theta2f} & g_{A3\theta2m} \end{bmatrix} \begin{Bmatrix} f_{A2} \\ m_{A2} \end{Bmatrix} + \begin{bmatrix} g_{A3x1f} & g_{A3x1m} \\ g_{A3\theta1f} & g_{A3\theta1m} \end{bmatrix} \begin{Bmatrix} f_{A1} \\ m_{A1} \end{Bmatrix} \tag{7}$$

where x_{ki} and θ_{ki} represent the translational and rotational displacements, respectively. f_{ki} and m_{ki} are the applied force and moment. The subscript k refers to the substructure (i.e., *SH*, *T*) or assembly (i.e., *A*). g_{kij} is the receptance between point i and j. The second subscript is the response point and the third one is the exciting point.

The compatibility and equilibrium conditions for such substructure layout are given by, respectively,

$$\begin{cases} x_{SH3} = x_{T3} = x_{A3} \\ x_{T1} = x_{A1}, \quad x_{T2} = x_{A2} \\ \theta_{SH3} = \theta_{T3} = \theta_{A3} \\ \theta_{T1} = \theta_{A1}, \quad \theta_{T2} = \theta_{A2} \end{cases} \tag{8}$$

$$\begin{cases} f_{A3} = f_{SH3} + f_{T3} \\ f_{T1} = f_{A1}, \quad f_{T2} = f_{A2} \\ m_{A3} = m_{SH3} + m_{T3} \\ m_{T1} = m_{A1}, \quad m_{T2} = m_{A2} \end{cases} \tag{9}$$

Introducing the receptance functions of substructure *SH* and *T* in the corresponding compatibility condition at point 3 leads to

$$\begin{bmatrix} g_{SH3x3f} & g_{SH3x3m} \\ g_{SH3\theta3f} & g_{SH3\theta3m} \end{bmatrix} \begin{Bmatrix} f_{SH3} \\ m_{SH3} \end{Bmatrix} = \begin{bmatrix} g_{T3x3f} & g_{T3x3m} \\ g_{T3\theta3f} & g_{T3\theta3m} \end{bmatrix} \begin{Bmatrix} f_{T3} \\ m_{T3} \end{Bmatrix} + \begin{bmatrix} g_{T3x2f} & g_{T3x2m} \\ g_{T3\theta2f} & g_{T3\theta2m} \end{bmatrix} \begin{Bmatrix} f_{T2} \\ m_{T2} \end{Bmatrix} + \begin{bmatrix} g_{T3x1f} & g_{T3x1m} \\ g_{T3\theta1f} & g_{T3\theta1m} \end{bmatrix} \begin{Bmatrix} f_{T1} \\ m_{T1} \end{Bmatrix} \tag{10}$$

By substituting the equilibrium condition into Eq. (10), the following relation can be obtained:

$$\begin{bmatrix} g_{SH3x3f} + g_{T3x3f} & g_{SH3x3m} + g_{T3x3m} \\ g_{SH3\theta3f} + g_{T3\theta3f} & g_{SH3\theta3m} + g_{T3\theta3m} \end{bmatrix} \begin{Bmatrix} f_{T3} \\ m_{T3} \end{Bmatrix} = \begin{bmatrix} g_{SH3x3f} & g_{SH3x3m} \\ g_{SH3\theta3f} & g_{SH3\theta3m} \end{bmatrix} \begin{Bmatrix} f_{A3} \\ m_{A3} \end{Bmatrix} - \begin{bmatrix} g_{T3x2f} & g_{T3x2m} \\ g_{T3\theta2f} & g_{T3\theta2m} \end{bmatrix} \begin{Bmatrix} f_{A2} \\ m_{A2} \end{Bmatrix} - \begin{bmatrix} g_{T3x1f} & g_{T3x1m} \\ g_{T3\theta1f} & g_{T3\theta1m} \end{bmatrix} \begin{Bmatrix} f_{A1} \\ m_{A1} \end{Bmatrix} \tag{11}$$

The loads of substructure *T* at point 3 are then expressed as

$$\begin{cases} f_{T3} = c_1 f_{A1} + c_2 f_{A2} + c_3 f_{A3} + c_4 m_{A1} + c_5 m_{A2} + c_6 m_{A3} \\ m_{T3} = c_7 f_{A1} + c_8 f_{A2} + c_9 f_{A3} + c_{10} m_{A1} + c_{11} m_{A2} + c_{12} m_{A3} \end{cases} \tag{12}$$

where c_1~c_{12} are coefficients which are closely related to the receptance matrix terms in Eq. (11) (see Appendix).

Similarly, for substructures *T* and *A*, the compatibility and equilibrium conditions at points 1, 2, and 3 can provide the following equation:

$$\begin{bmatrix} g_{A1x3f} & g_{A1x3m} & g_{A1x2f} & g_{A1x2m} & g_{A1x1f} & g_{A1x1m} \\ g_{A1\theta3f} & g_{A1\theta3m} & g_{A1\theta2f} & g_{A1\theta2m} & g_{A1\theta1f} & g_{A1\theta1m} \\ g_{A2x3f} & g_{A2x3m} & g_{A2x2f} & g_{A2x2m} & g_{A2x1f} & g_{A2x1m} \\ g_{A2\theta3f} & g_{A2\theta3m} & g_{A2\theta2f} & g_{A2\theta2m} & g_{A2\theta1f} & g_{A2\theta1m} \\ g_{A3x3f} & g_{A3x3m} & g_{A3x2f} & g_{A3x2m} & g_{A3x1f} & g_{A3x1m} \\ g_{A3\theta3f} & g_{A3\theta3m} & g_{A3\theta2f} & g_{A3\theta2m} & g_{A3\theta1f} & g_{A3\theta1m} \end{bmatrix} \begin{Bmatrix} f_{A3} \\ m_{A3} \\ f_{A2} \\ m_{A2} \\ f_{A1} \\ m_{A1} \end{Bmatrix} = \begin{bmatrix} g_{T1x3f} & g_{T1x3m} & g_{T1x2f} & g_{T1x2m} & g_{T1x1f} & g_{T1x1m} \\ g_{T1\theta3f} & g_{T1\theta3m} & g_{T1\theta2f} & g_{T1\theta2m} & g_{T1\theta1f} & g_{T1\theta1m} \\ g_{T2x3f} & g_{T2x3m} & g_{T2x2f} & g_{T2x2m} & g_{T2x1f} & g_{T2x1m} \\ g_{T2\theta3f} & g_{T2\theta3m} & g_{T2\theta2f} & g_{T2\theta2m} & g_{T2\theta1f} & g_{T2\theta1m} \\ g_{T3x3f} & g_{T3x3m} & g_{T3x2f} & g_{T3x2m} & g_{T3x1f} & g_{T3x1m} \\ g_{T3\theta3f} & g_{T3\theta3m} & g_{T3\theta2f} & g_{T3\theta2m} & g_{T3\theta1f} & g_{T3\theta1m} \end{bmatrix} \begin{Bmatrix} f_{T3} \\ m_{T3} \\ f_{A2} \\ m_{A2} \\ f_{A1} \\ m_{A1} \end{Bmatrix} \tag{13}$$

Substituting Eq. (12) into Eq. (13) yields

$$\begin{bmatrix} g_{A1x3f} & g_{A1x3m} & g_{A1x2f} & g_{A1x2m} & g_{A1x1f} & g_{A1x1m} \\ g_{A1\theta3f} & g_{A1\theta3m} & g_{A1\theta2f} & g_{A1\theta2m} & g_{A1\theta1f} & g_{A1\theta1m} \\ g_{A2x3f} & g_{A2x3m} & g_{A2x2f} & g_{A2x2m} & g_{A2x1f} & g_{A2x1m} \\ g_{A2\theta3f} & g_{A2\theta3m} & g_{A2\theta2f} & g_{A2\theta2m} & g_{A2\theta1f} & g_{A2\theta1m} \\ g_{A3x3f} & g_{A3x3m} & g_{A3x2f} & g_{A3x2m} & g_{A3x1f} & g_{A3x1m} \\ g_{A3\theta3f} & g_{A3\theta3m} & g_{A3\theta2f} & g_{A3\theta2m} & g_{A3\theta1f} & g_{A3\theta1m} \end{bmatrix} \begin{Bmatrix} f_{A3} \\ m_{A3} \\ f_{A2} \\ m_{A2} \\ f_{A1} \\ m_{A1} \end{Bmatrix} = \begin{bmatrix} g_{T1x3f} & g_{T1x3m} & g_{T1x2f} & g_{T1x2m} & g_{T1x1f} & g_{T1x1m} \\ g_{T1\theta3f} & g_{T1\theta3m} & g_{T1\theta2f} & g_{T1\theta2m} & g_{T1\theta1f} & g_{T1\theta1m} \\ g_{T2x3f} & g_{T2x3m} & g_{T2x2f} & g_{T2x2m} & g_{T2x1f} & g_{T2x1m} \\ g_{T2\theta3f} & g_{T2\theta3m} & g_{T2\theta2f} & g_{T2\theta2m} & g_{T2\theta1f} & g_{T2\theta1m} \\ g_{T3x3f} & g_{T3x3m} & g_{T3x2f} & g_{T3x2m} & g_{T3x1f} & g_{T3x1m} \\ g_{T3\theta3f} & g_{T3\theta3m} & g_{T3\theta2f} & g_{T3\theta2m} & g_{T3\theta1f} & g_{T3\theta1m} \end{bmatrix} \begin{Bmatrix} c_1 f_{A1} + c_2 f_{A2} + c_3 f_{A3} + c_4 m_{A1} + c_5 m_{A2} + c_6 m_{A3} \\ c_7 f_{A1} + c_8 f_{A2} + c_9 f_{A3} + c_{10} m_{A1} + c_{11} m_{A2} + c_{12} m_{A3} \\ f_{A2} \\ m_{A2} \\ f_{A1} \\ m_{A1} \end{Bmatrix} \tag{14}$$

Regrouping the corresponding terms of Eq. (14) leads to

$$
\begin{bmatrix}
g_{A1x3f}f_{A3}+g_{A1x3m}m_{A3}+g_{A1x2f}f_{A2}+g_{A1x2m}m_{A2}+g_{A1x1f}f_{A1}+g_{A1x1m}m_{A1}\\
g_{A1\theta3f}f_{A3}+g_{A1\theta3m}m_{A3}+g_{A1\theta2f}f_{A2}+g_{A1\theta2m}m_{A2}+g_{A1\theta1f}f_{A1}+g_{A1\theta1m}m_{A1}\\
g_{A2x3f}f_{A3}+g_{A2x3m}m_{A3}+g_{A2x2f}f_{A2}+g_{A2x2m}m_{A2}+g_{A2x1f}f_{A1}+g_{A2x1m}m_{A1}\\
g_{A2\theta3f}f_{A3}+g_{A2\theta3m}m_{A3}+g_{A2\theta2f}f_{A2}+g_{A2\theta2m}m_{A2}+g_{A2\theta1f}f_{A1}+g_{A2\theta1m}m_{A1}\\
g_{A3x3f}f_{A3}+g_{A3x3m}m_{A3}+g_{A3x2f}f_{A2}+g_{A3x2m}m_{A2}+g_{A3x1f}f_{A1}+g_{A3x1m}m_{A1}\\
g_{A3\theta3f}f_{A3}+g_{A3\theta3m}m_{A3}+g_{A3\theta2f}f_{A2}+g_{A3\theta2m}m_{A2}+g_{A3\theta1f}f_{A1}+g_{A3\theta1m}m_{A1}
\end{bmatrix}=
$$

$$
\begin{bmatrix}
\left(c_3g_{T1x3f}+c_9g_{T1x3m}\right)f_{A3}+\left(c_6g_{T1x3f}+c_{12}g_{T1x3m}\right)m_{A3}+\left(c_2g_{T1x3f}+c_8g_{T1x3m}+g_{T1x2f}\right)f_{A2}+\\
\left(c_3g_{T1\theta3f}+c_9g_{T1\theta3m}\right)f_{A3}+\left(c_6g_{T1\theta3f}+c_{12}g_{T1\theta3m}\right)m_{A3}+\left(c_2g_{T1\theta3f}+c_8g_{T1\theta3m}+g_{T1\theta2f}\right)f_{A2}+\\
\left(c_3g_{T2x3f}+c_9g_{T2x3m}\right)f_{A3}+\left(c_6g_{T2x3f}+c_{12}g_{T2x3m}\right)m_{A3}+\left(c_2g_{T2x3f}+c_8g_{T2x3m}+g_{T2x2f}\right)f_{A2}+\\
\left(c_3g_{T2\theta3f}+c_9g_{T2\theta3m}\right)f_{A3}+\left(c_6g_{T2\theta3f}+c_{12}g_{T2\theta3m}\right)m_{A3}+\left(c_2g_{T2\theta3f}+c_8g_{T2\theta3m}+g_{T2\theta2f}\right)f_{A2}+\\
\left(c_3g_{T3x3f}+c_9g_{T3x3m}\right)f_{A3}+\left(c_6g_{T3x3f}+c_{12}g_{T3x3m}\right)m_{A3}+\left(c_2g_{T3x3f}+c_8g_{T3x3m}+g_{T3x2f}\right)f_{A2}+\\
\left(c_3g_{T3\theta3f}+c_9g_{T3\theta3m}\right)f_{A3}+\left(c_6g_{T3\theta3f}+c_{12}g_{T3\theta3m}\right)m_{A3}+\left(c_2g_{T3\theta3f}+c_8g_{T3\theta3m}+g_{T3\theta2f}\right)f_{A2}+\\
\left(c_5g_{T1x3f}+c_{11}g_{T1x3m}+g_{T1x2m}\right)m_{A2}+\left(c_1g_{T1x3f}+c_7g_{T1x3m}+g_{T1x1f}\right)f_{A1}+\left(c_4g_{T1x3f}+c_{10}g_{T1x3m}+g_{T1x1m}\right)m_{A1}\\
\left(c_5g_{T1\theta3f}+c_{11}g_{T1\theta3m}+g_{T1\theta2m}\right)m_{A2}+\left(c_1g_{T1\theta3f}+c_7g_{T1\theta3m}+g_{T1\theta1f}\right)f_{A1}+\left(c_4g_{T1\theta3f}+c_{10}g_{T1\theta3m}+g_{T1\theta1m}\right)m_{A1}\\
\left(c_5g_{T2x3f}+c_{11}g_{T2x3m}+g_{T2x2m}\right)m_{A2}+\left(c_1g_{T2x3f}+c_7g_{T2x3m}+g_{T2x1f}\right)f_{A1}+\left(c_4g_{T2x3f}+c_{10}g_{T2x3m}+g_{T2x1m}\right)m_{A1}\\
\left(c_5g_{T2\theta3f}+c_{11}g_{T2\theta3m}+g_{T2\theta2m}\right)m_{A2}+\left(c_1g_{T2\theta3f}+c_7g_{T2\theta3m}+g_{T2\theta1f}\right)f_{A1}+\left(c_4g_{T2\theta3f}+c_{10}g_{T2\theta3m}+g_{T2\theta1m}\right)m_{A1}\\
\left(c_5g_{T3x3f}+c_{11}g_{T3x3m}+g_{T3x2m}\right)m_{A2}+\left(c_1g_{T3x3f}+c_7g_{T3x3m}+g_{T3x1f}\right)f_{A1}+\left(c_4g_{T3x3f}+c_{10}g_{T3x3m}+g_{T3x1m}\right)m_{A1}\\
\left(c_5g_{T3\theta3f}+c_{11}g_{T3\theta3m}+g_{T3\theta2m}\right)m_{A2}+\left(c_1g_{T3\theta3f}+c_7g_{T3\theta3m}+g_{T3\theta1f}\right)f_{A1}+\left(c_4g_{T3\theta3f}+c_{10}g_{T3\theta3m}+g_{T3\theta1m}\right)m_{A1}
\end{bmatrix}
\tag{15}
$$

According to the equivalent coefficients of the corresponding terms in the matrix of Eq. (15), we can obtain the following equations:

$$
\begin{cases}
g_{A1x3f}=c_3g_{T1x3f}+c_9g_{T1x3m}\\
g_{A1x2f}=c_2g_{T1x3f}+c_8g_{T1x3m}+g_{T1x2f}\\
g_{A1x1f}=c_1g_{T1x3f}+c_7g_{T1x3m}+g_{T1x1f}\\
g_{A2x1f}=c_1g_{T2x3f}+c_7g_{T2x3m}+g_{T2x1f}\\
g_{A3x1f}=c_1g_{T3x3f}+c_7g_{T3x3m}+g_{T3x1f}\\
g_{A2x3f}=c_3g_{T2x3f}+c_9g_{T2x3m}\\
g_{A3x2f}=c_2g_{T3x3f}+c_8g_{T3x3m}+g_{T3x2f}
\end{cases}
\tag{16}
$$

By reciprocity, the following equations must be fulfilled:

$$
\begin{cases}
g_{A1x3f}=g_{A3x1f}\\
g_{A1x2f}=g_{A2x1f}\\
g_{A2x3f}=g_{A3x2f}
\end{cases}
\tag{17}
$$

Substituting corresponding equations of Eq. (16) into Eq. (17) leads to

$$
\begin{cases}
c_3g_{T1x3f}+c_9g_{T1x3m}=g_{A1x3f}\\
c_2g_{T1x3f}+c_8g_{T1x3m}=g_{A1x2f}-g_{T1x2f}\\
c_1g_{T1x3f}+c_7g_{T1x3m}=g_{A1x1f}-g_{T1x1f}\\
c_1g_{T3x3f}+c_7g_{T3x3m}-c_3g_{T1x3f}-c_9g_{T1x3m}=-g_{T3x1f}\\
c_1g_{T2x3f}+c_7g_{T2x3m}-c_2g_{T1x3f}-c_8g_{T1x3m}=0\\
c_2g_{T3x3f}+c_8g_{T3x3m}-c_3g_{T2x3f}-c_9g_{T2x3m}=-g_{T3x2f}
\end{cases}
\tag{18}
$$

Equation (18) can be rewritten in matrix form as

$$
\begin{bmatrix}
0 & 0 & 0 & 0 & g_{T1x3f} & g_{T1x3m}\\
0 & 0 & g_{T1x3f} & g_{T1x3m} & 0 & 0\\
g_{T1x3f} & g_{T1x3m} & 0 & 0 & 0 & 0\\
g_{T3x3f} & g_{T3x3m} & 0 & 0 & -g_{T1x3f} & -g_{T1x3m}\\
g_{T2x3f} & g_{T2x3m} & -g_{T1x3f} & -g_{T1x3m} & 0 & 0\\
0 & 0 & g_{T3x3f} & g_{T3x3m} & -g_{T2x3f} & -g_{T2x3m}
\end{bmatrix}
\begin{bmatrix}c_1\\c_7\\c_2\\c_8\\c_3\\c_9\end{bmatrix}=
\begin{bmatrix}
g_{A3x1f}\\
g_{A2x1f}-g_{T1x2f}\\
g_{A1x1f}-g_{T1x1f}\\
-g_{T3x1f}\\
0\\
-g_{T3x2f}
\end{bmatrix}
\tag{19}
$$

Equation (19) is a non-homogeneous linear equation and the determinant of its coefficient matrix is zero, so Eq. (19) has no unique solution. Nevertheless, c_1 and c_7 can be solved using the third and fourth equations in Eq. (16), as shown in Eq. (20).

$$\begin{bmatrix} g_{T1x3f} & g_{T1x3m} \\ g_{T2x3f} & g_{T2x3m} \end{bmatrix} \begin{bmatrix} c_1 \\ c_7 \end{bmatrix} = \begin{bmatrix} g_{A1x1f} - g_{T1x1f} \\ g_{A2x1f} - g_{T2x1f} \end{bmatrix} \tag{20}$$

The assembly receptances g_{A2x1f} and g_{A1x1f} can be experimentally identified through an impact test, and the tool receptances can be obtained using the finite element method. Therefore, the unknowns (c_1 and c_7) can be calculated by solving Eq. (20).

Similarly, substituting Eq. (12) into Eq. (11) and regrouping the corresponding terms leads to

$$\begin{cases} c_1 g_{SH3x3f} + c_7 g_{SH3x3m} = -g_{T3x1f} - c_1 g_{T3x3f} - c_7 g_{T3x3m} \\ c_1 g_{SH3\theta3f} + c_7 g_{SH3\theta3m} = -g_{T3\theta1f} - c_1 g_{T3\theta3f} - c_7 g_{T3\theta3m} \end{cases} \tag{21}$$

There are four unknowns in Eq. (21); it is impossible to directly solve it. Note that g_{SH3x3m} is equal to $g_{SH3\theta3f}$ due to reciprocity, and $g_{SH3\theta3m}$ can be calculated from g_{SH3x3m}, $g_{SH3\theta3f}$, and g_{SH3x3f} [16], as shown in Eq. (22).

$$g_{SH3\theta3m} = \frac{\theta_{SH3}}{m_{SH3}} = \frac{f_{SH3}\, x_{SH3}\, \theta_{SH3}}{x_{SH3}\, m_{SH3} f_{SH3}} = \frac{g_{SH3x3m} g_{SH3\theta3f}}{g_{SH3x3f}} = \frac{(g_{SH3x3m})^2}{g_{SH3x3f}} \tag{22}$$

Based on the two sets of equations (Eqs. (21) and (22)), all the substructure *SH* receptance components can then be obtained as

$$\begin{cases} g_{SH3x3m} = g_{SH3\theta3f} = \dfrac{\left(-g_{T3x1f} - c_1 g_{T3x3f} - c_7 g_{T3x3m}\right)\left(-g_{T3\theta1f} - c_1 g_{T3\theta3f} - c_7 g_{T3\theta3m}\right)}{c_1\left(-g_{T3x1f} - c_1 g_{T3x3f} - c_7 g_{T3x3m}\right) + c_7\left(-g_{T3\theta1f} - c_1 g_{T3\theta3f} - c_7 g_{T3\theta3m}\right)} \\ g_{SH3x3f} = \dfrac{\left(-g_{T3x1f} - c_1 g_{T3x3f} - c_7 g_{T3x3m}\right) - c_7 g_{SH3\theta3f}}{c_1} \\ g_{SH3\theta3m} = \dfrac{\left(-g_{T3\theta1f} - c_1 g_{T3\theta3f} - c_7 g_{T3\theta3m}\right) - c_1 g_{SH3\theta3f}}{c_7} \end{cases} \tag{23}$$

After obtaining all the translational and rotational dynamics of substructure *SH*, the tool point FRF can be identified by analytically coupling them with any attached free-free tool dynamics using the traditional RCSA method.

From the above analysis, it is observed that coupling joint (point 3) receptances can be calculated from experimental FRFs related to additional point (point 2) and tool point (point 1). Compared to the present state of the art, the main improvements of the proposed method are as follows:

1. Actually, there are only two independent variables in the coupling joint receptances matrix (i.e.,g_{SH3x3m}, g_{SH3x3f}, $g_{SH3\theta3f}$, and $g_{SH3\theta3m}$) according to reference [16]. Two receptance inputs are enough to obtain all receptance components. Only two accelerometers are needed under the condition of one impact. Although one accelerometer and two impacts can also be used to complete the experiments, the measurement time will be considerable for the case of an enormous number of tool/holder/spindle combinations. The proposed method adopts two accelerometers and one impact to reduce hammer impact times, further increasing the prediction efficiency compared to the methods proposed in [21, 24].
2. Enough room should be reserved for the impact hammering and accelerometer installation. In some cases, impact testing cannot be performed on the coupling joint point by the methods proposed in [21, 24] due to space limitation. In the proposed method, only the tool point is impacted, separating the coupling joint point to avoid impact hammering and accelerometer installation. If a mini-accelerometer or ultra-miniature accelerometer is adopted to record the vibration signals, the joint location can be placed to the holder nose as close as possible. Therefore, a wider range of tool length for the tool point FRF prediction can be achieved.

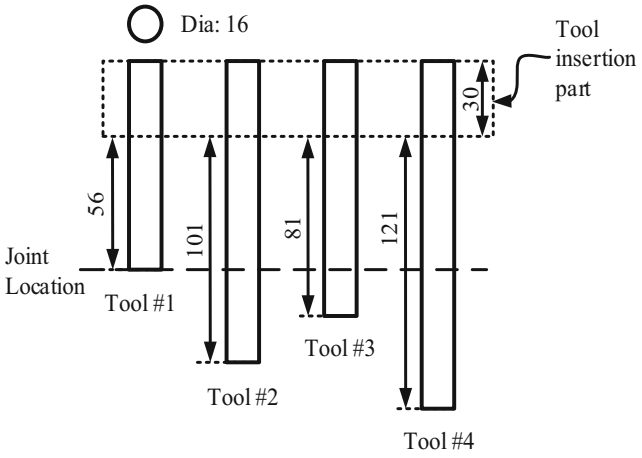

Fig. 2 Cylindrical blanks used in the experiments

3 Experimental verification

To verify the proposed method, experiments were performed on a self-designed setup for the 170XDS20Z11 spindle system equipped with a HSK-ER40 holder with 16 mm collect. Four steel blanks with the same diameter of 16 mm but different lengths were tested, as shown in Fig. 2. Tool no. 1 and no. 2 are used to obtain the necessary information required by Park's method [21]. Tool no. 2 is used to calculate substructure *SH* dynamics by adopting Montevecchi's method [24] and the proposed method, respectively. Tool no. 3 and no. 4 are used to validate the proposed approach, as well as to compare to the existing techniques. The elastic modulus of the blanks is 210 GPa, and the mass density and Poisson's ratio are 7850 kg/m^3 and 0.3, respectively. The tool insertion length is maintained at 30 mm in all cases.

In the proposed method, hammering impact was conducted at the tool point through a PCB 086C01 impact hammer. Two mini-accelerometers (B&W 14236, mass 1.9 g) were placed at the additional point location (accelerometer no. 2) and tool point location (accelerometer no. 1) to record the resulting vibration responses. The distance between the tool point location and additional point location is 20 mm, and that between the additional point location and coupling joint location is 25 mm, as shown in Fig. 3. Both impact and vibration signals were collected by the LMS SCADAS Mobile system and analyzed by LMS Test Lab software. To reduce random error, the average result of five impacts was adopted in each case. Besides, the mass loading effect of accelerometers on FRFs is neglected due to low accelerometer-to-tool mass ratio [25] in this paper.

Only the direct receptance g_{A1x1f} and cross receptance g_{A2x1f} are required by the proposed approach, and the information related to the coupling joint (point 3) is not necessary. Figure 4 shows these two measured FRFs.

The common options to compute the free-free tool dynamics include finite element method and closed-form expressions for uniform Timoshenko beam or Euler-Bernoulli beam. Previous research [11] has shown that Timoshenko beam theory is more accurate than Euler-Bernoulli beam theory in FRF prediction. The Timoshenko beam model is adopted to develop the free-free tool receptances in this case. Once obtaining these free-free tool receptances, the coupling joint dynamics can be calculated by the proposed method. Figure 5 compares the rotational-rotational receptance and translational-rotational cross receptance at the coupling joint location (point 3), which are extracted from different approaches. Significant differences can be observed among these methods. Park's method shows an obvious peak around 870 Hz in rotational-rotational receptance, which is not clear in other two methods. The main reason for the discrepancies may be that each method adopts different inputs and

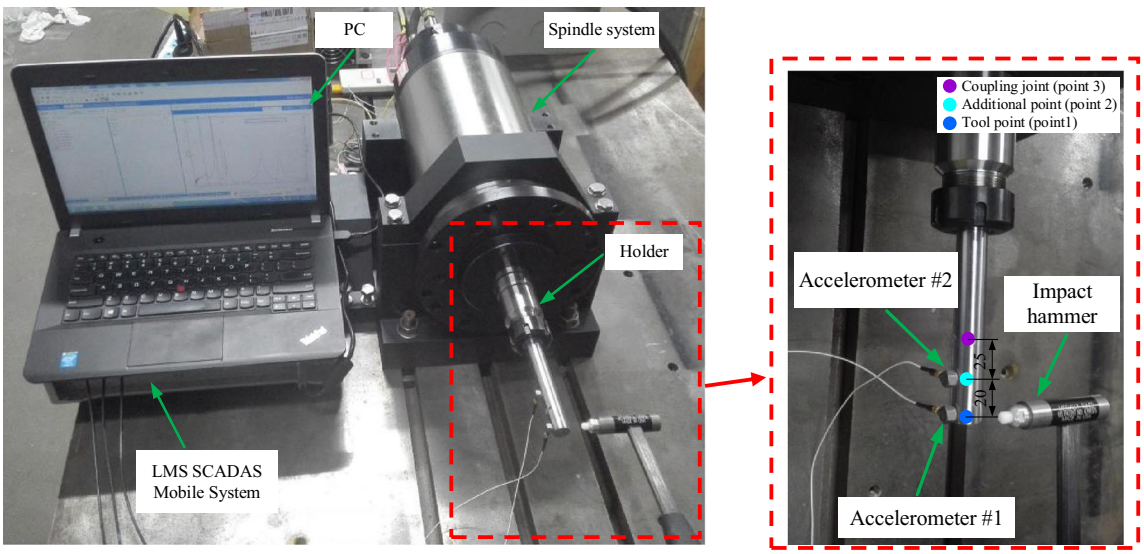

Fig. 3 Experimental setup

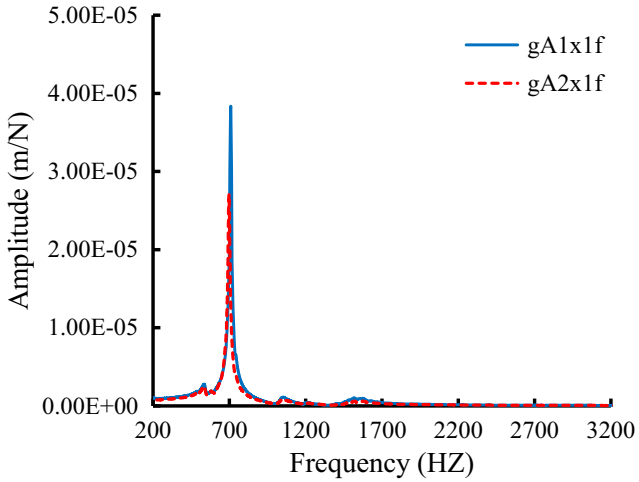

Fig. 4 Experimental FRFs required by the proposed method

algorithms to calculate these receptances and handles the measurement noise in different ways.

Based on the calculated coupling joint receptances and free-free tool dynamics, the tool point FRF can be evaluated using the traditional RCSA technique. Two blanks with different lengths (i.e., tool no. 3 and no. 4) are selected for the verification of the proposed method.

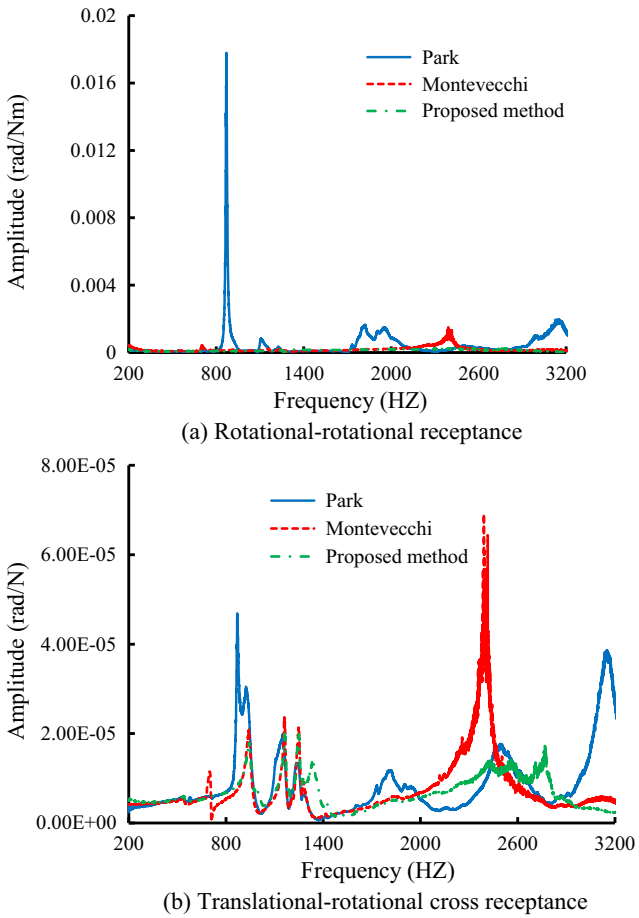

Fig. 5 Coupling joint receptances extracted from different methods. **a** Rotational-rotational receptance. **b** Translational-rotational cross receptance

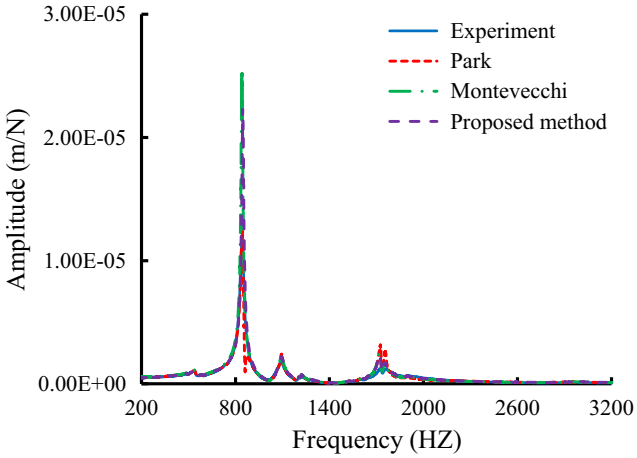

Fig. 6 Tool point FRF predictions for tool no. 3

Tool no. 3 results are plotted in Fig. 6, in which the predictions obtained via different approaches and the measurements are given for comparisons. It can be seen that the predicted FRF using the proposed method agrees well with the measured one, except for a difference in amplitude on the second dominant mode (around 846 Hz). Besides, the amplitude values around the second dominant mode is the highest for Montevecchi's method and results obtained from Park's method deviate far from the measurements at around 860 Hz. These small discrepancies between predictions and experimental results are attributed to noises in measurement data. The coupling joint receptance matrix is obtained by inverse receptance coupling technique; the measurement noise effect can be considered to be amplified. The tool point FRF is calculated through receptance coupling method, which is an inverse procedure of coupling joint receptance solution; the noise effect is thought to be reduced, and vice versa. Figure 7 shows the tool point FRF predictions for tool no. 4. Good

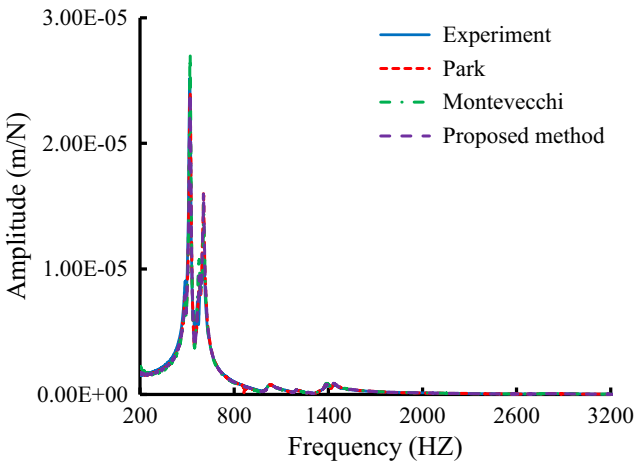

Fig. 7 Tool point FRF predictions for tool no. 4

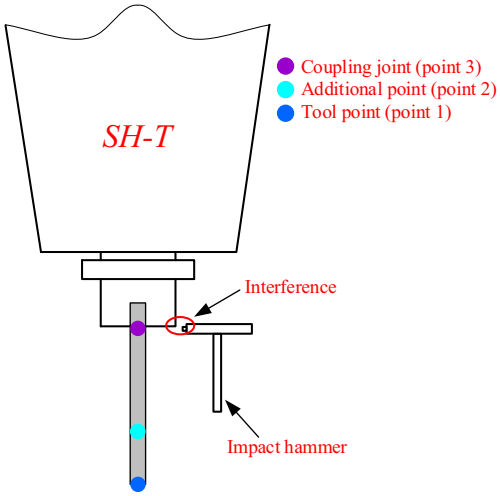

Fig. 8 Hammer impact interference at coupling joint by Montevecchi's method [24]

agreement between predicted FRFs and experimental results is also observed.

Unlike the method proposed by Montevecchi [24], it is not necessary to conduct impacts and install an accelerometer at the coupling joint location. Generally, if the mini-accelerometer or ultra-miniature accelerometer is used, the room which is required by the impact hammering is larger than the size of the accelerometer. When the holder nose point is needed to be impacted, an interference between the impact hammer and holder will appear, resulting in the failure to obtain the coupling joint receptances, as shown in Fig. 8. However, coupling joint location (i.e., point 3 in this case) can be placed to the holder nose as close as possible by the proposed method, and then a wider range of tool length for tool point FRF prediction can be achieved. Besides, if the holder-tool contact dynamics are available, the coupling joint can even be placed at the spindle nose, then the proposed method can be used to determine tool point FRF for a wide range of different types of holder and tool without the need to conduct an impact on every tool. In brief, the proposed method separates the coupling joint point to avoid an impact on it, and a wider application of the proposed method in predicting tool point FRF can be achieved than the state-of-the-art techniques.

4 Conclusions

In this paper, an efficient method to predict tool point dynamic was proposed. The rotational dynamics of the spindle-holder assembly were identified through an improved receptance coupling method. The required translational FRFs were obtained by two accelerometers with only one impact testing. The full receptance matrix of the spindle-holder assembly was then coupled with any attached free-free tool dynamics to predict tool point FRF. Experiments indicate that the presented approach can acquire the same accuracy in prediction with the state-of-the-art approaches. The main improvements of the proposed method are increasing prediction efficiency and obtaining a wider range of tool length for tool point FRF prediction. The proposed method can quickly and accurately identify tool point FRF for chatter prediction in milling operations.

Acknowledgements We gratefully acknowledge the financial support from the National Natural Science Foundation of China (Grant No. 51575301), the Key National Science and Technology Projects of China (Grant No. 2015ZX04014021), and the National Basic Research Program of China (Grant No. 2013CB035402).

Appendix. Expressions of c_1~c_{12}

The expressions of c_1~c_{12} can be obtained by solving Eq. (11). To simplify the expressions, we define the following equation:

$$K=\left(g_{SH3x3f}+g_{T3x3f}\right)\left(g_{SH3\theta3m}+g_{T3\theta3m}\right)-\left(g_{SH3x3m}+g_{T3x3m}\right)\left(g_{SH3\theta3f}+g_{T3\theta3f}\right) \tag{A1}$$

Then, these coefficients are given by, respectively

$$c_1=\frac{g_{T3\theta1f}\left(g_{SH3x3m}+g_{T3x3m}\right)-g_{T3x1f}\left(g_{SH3\theta3m}+g_{T3\theta3m}\right)}{K} \tag{A2}$$

$$c_2=\frac{g_{T3\theta2f}\left(g_{SH3x3m}+g_{T3x3m}\right)-g_{T3x2f}\left(g_{SH3\theta3m}+g_{T3\theta3m}\right)}{K} \tag{A3}$$

$$c_3=\frac{g_{SH3x3f}\left(g_{SH3\theta3m}+g_{T3\theta3m}\right)-g_{SH3\theta3f}\left(g_{SH3x3m}+g_{T3x3m}\right)}{K} \tag{A4}$$

$$c_4=\frac{g_{T3\theta1m}\left(g_{SH3x3m}+g_{T3x3m}\right)-g_{T3x1m}\left(g_{SH3\theta3m}+g_{T3\theta3m}\right)}{K} \tag{A5}$$

$$c_5=\frac{g_{T3\theta2m}\left(g_{SH3x3m}+g_{T3x3m}\right)-g_{T3x2m}\left(g_{SH3\theta3m}+g_{T3\theta3m}\right)}{K} \tag{A6}$$

$$c_6=\frac{g_{SH3x3m}\left(g_{SH3\theta3m}+g_{T3\theta3m}\right)-g_{SH3\theta3m}\left(g_{SH3x3m}+g_{T3x3m}\right)}{K} \tag{A7}$$

$$c_7=\frac{g_{T3x1f}\left(g_{SH3\theta3f}+g_{T3\theta3f}\right)-g_{T3\theta1f}\left(g_{SH3x3f}+g_{T3x3f}\right)}{K} \tag{A8}$$

$$c_8 = \frac{g_{T3x2f}\left(g_{SH3\theta3f} + g_{T3\theta3f}\right) - g_{T3\theta2f}\left(g_{SH3x3f} + g_{T3x3f}\right)}{K} \tag{A9}$$

$$c_9 = \frac{g_{SH3\theta3f}\left(g_{SH3x3f} + g_{T3x3f}\right) - g_{SH3x3f}\left(g_{SH3\theta3f} + g_{T3\theta3f}\right)}{K} \tag{A10}$$

$$c_{10} = \frac{g_{T3x1m}\left(g_{SH3\theta3f} + g_{T3\theta3f}\right) - g_{T3\theta1m}\left(g_{SH3x3f} + g_{T3x3f}\right)}{K} \tag{A11}$$

$$c_{11} = \frac{g_{T3x2m}\left(g_{SH3\theta3f} + g_{T3\theta3f}\right) - g_{T3\theta2m}\left(g_{SH3x3f} + g_{T3x3f}\right)}{K} \tag{A12}$$

$$c_{12} = \frac{g_{SH3\theta3m}\left(g_{SH3x3f} + g_{T3x3f}\right) - g_{SH3x3m}\left(g_{SH3\theta3f} + g_{T3\theta3f}\right)}{K} \tag{A13}$$

References

1. Movahhedy MR, Gerami JM (2006) Prediction of spindle dynamics in milling by sub-structure coupling. Int J Mach Tools Manuf 46(3):243–251
2. Xu C, Zhang JF, Yu DW, Wu ZJ, Feng PF (2015) Dynamics prediction of spindle system using joint models of spindle tool holder and bearings. Proc Inst Mech Eng C J Mech Eng Sci 229(17):3084–3095
3. Xu C, Feng PF, Zhang JF, Yu DW, Wu ZJ (2017) Milling stability prediction for flexible workpiece using dynamics of coupled machining system. Int J Adv Manuf Technol 90(9–12):3217–3227
4. Liao JP, Zhang JF, Feng PF, Yu DW, Wu ZJ (2017) Identification of contact stiffness of shrink-fit tool-holder joint based on fractal theory. Int J Adv Manuf Technol 90(5–8):2173–2184
5. Duncan GS, Tummond MF, Schmitz TL (2005) An investigation of the dynamic absorber effect in high-speed machining. Int J Mach Tools Manuf 45(4–5):497–507
6. Li ZQ, Wang ZK, Shi XF (2017) Fast prediction of chatter stability lobe diagram for milling process using frequency response function or modal parameters. Int J Adv Manuf Technol 89(9–12):2603–2612
7. Ewins DJ (2000) Modal testing: theory, practice and application, 2nd edn. Research Studies Press, England
8. Schmitz TL, Davies MA, Kennedy MD (2001) Tool point frequency response prediction for high-speed machining by RCSA. J Manuf Sci E T ASME 123(4):700–707
9. Özşahin O, Altintas Y (2015) Prediction of frequency response function (FRF) of asymmetric tools from the analytical coupling of spindle and beam models of holder and tool. Int J Mach Tools Manuf 92:31–40
10. Filiz S, Cheng CH, Powell KB, Schmitz TL, Ozdoganlar OB (2009) An improved tool–holder model for RCSA tool-point frequency response prediction. Precis Eng 33(1):26–36
11. Ertürk A, Özgüven HN, Budak E (2006) Analytical modeling of spindle–tool dynamics on machine tools using Timoshenko beam model and receptance coupling for the prediction of tool point FRF. Int J Mach Tools Manuf 46(15):1901–1912
12. Zhang J, Schmitz T, Zhao WH, Lu BH (2011) Receptance coupling for tool point dynamics prediction on machine tools. Chin J Mech Eng 24(3):340–345
13. Kivanc EB, Budak E (2004) Structural modeling of end mills for form error and stability analysis. Int J Mach Tools Manuf 44(11):1151–1161
14. Duarte MLM, Ewins DJ (2000) Rotational degrees of freedom for structural coupling analysis via finite-difference technique with residual compensation. Mech Syst Signal Process 14(2):205–227
15. Liu Z, Song XL, Zhao YS, Cai LG, Guo HS, Ma JC (2013) Stiffness identification of spindle-toolholder joint based on finite difference technique and residual compensation theory. Adv Mech Eng 5:753631
16. Schmitz TL, Duncan GS (2005) Three-component receptance coupling substructure analysis for tool point dynamics prediction. J Manuf Sci E T ASME 127(4):781–790
17. Albertelli P, Goletti M, Monno M (2013) An improved receptance coupling substructure analysis to predict chatter free high speed cutting conditions. Procedia CIRP 12:19–24
18. Albertelli P, Goletti M, Monno M (2013) A new receptance coupling substructure analysis methodology to improve chatter free cutting conditions prediction. Int J Mach Tools Manuf 72:16–24
19. Kumar UV, Schmitz TL (2012) Spindle dynamics identification for receptance coupling substructure analysis. Precis Eng 36(3):435–443
20. Ganguly V, Schmitz TL (2013) Spindle dynamics identification using particle swarm optimization. J Manuf Process 15(4):444–451
21. Park SS, Altintas Y, Movahhedy M (2003) Receptance coupling for end mills. Int J Mach Tools Manuf 43(9):889–896
22. Mancisidor I, Urkiola A, Barcena R, Munoa J, Dombovari Z, Zatarain M (2014) Receptance coupling for tool point dynamic prediction by fixed boundaries approach. Int J Mach Tools Manuf 78:18–29
23. Park SS, Chae J (2008) Joint identification of modular tools using a novel receptance coupling method. Int J Adv Manuf Technol 35(11–12):1251–1262
24. Montevecchi F, Grossi N, Scippa A, Campatelli G (2016) Improved RCSA technique for efficient tool-tip dynamics prediction. Precis Eng 44:152–162
25. Özşahin O, Özgüven HN, Budak E (2010) Analysis and compensation of mass loading effect of accelerometers on tool point FRF measurements for chatter stability predictions. Int J Mach Tools Manuf 50(6):585–589